Pulsed Neutron Spectroscopic Imaging for Crystallographic Texture and Microstructure

Hirotaka Sato[a,*], Takashi Kamiyama[a], Kenji Iwase[b], Toru Ishigaki[b] and Yoshiaki Kiyanagi[a]

[a] Graduate School of Engineering, Hokkaido University, Sapporo 060-8628, Japan;
[b] Frontier Research Center for Applied Atomic Sciences, Ibaraki University, Ibaraki 319-1106, Japan.

*Corresponding author: Mr. Hirotaka Sato
hakuryu@eng.hokudai.ac.jp
Kita-13 Nishi-8, Kita-ku, Sapporo 060-8628, Japan.
Tel: +81-11-706 6652; Fax: +81-11-706 6652.

Abstract: A time-of-flight (TOF) spectroscopic neutron imaging at a pulsed neutron source is expected to be a new material analysis tool because this method can non-destructively investigate the spatial dependence of the crystallographic and metallographic information in a bulk material. For quantitative evaluation of such information, a spectral analysis code for the transmission data is necessary. Therefore, we have developed a Rietveld-like analysis code, RITS. Furthermore, we have applied the RITS code to evaluation of the position dependence of the crystal orientation anisotropy, the preferred orientation and the crystallite size of a welded α-iron plate, and we have successfully obtained the information on the texture and the microstructure. However, the reliability of the values given by the RITS code has not been evaluated yet in detail. For this reason, we compared the parameters provided by the RITS code with the parameters obtained by the neutron TOF powder diffractometry and its Rietveld analysis. Both the RITS code and the Rietveld analysis software indicated values close to each other, but there were systematic differences on the preferred orientation and the crystallite size.

Keywords: Bragg-edge transmission imaging; Rietveld analysis; Texture; Crystallite size; Neutron diffraction.

1. Introduction

Information on texture (crystal orientation anisotropy and preferred orientation) and microstructure (crystallite size) as well as strain and stress is very important for characterization of the metallurgical properties of structural or functional materials. In particular, the bulk information, which cannot be non-destructively investigated by EBSD (electron backscatter diffraction), X-ray diffraction and X-ray phase-contrast microtomography, reflects an essential property of the entire material. For exploration of such information, a time-of-flight (TOF) spectroscopic neutron imaging at a pulsed neutron source [1] is the most suitable technique because this method can give the position-dependent Bragg-edge transmission spectra over the wide area with a use of a neutron imaging detector, which include the texture and microstructure information of a bulk material at each pixel position. Therefore, a data analysis code for the Bragg-edge transmission spectrum is indispensable for the quantitative evaluation of the crystallographic and metallographic information. For this reason, we have developed a Rietveld-like analysis code, RITS (Rietveld Imaging of Transmission Spectra) [2,3], and we have successfully carried out the quantitative imaging of the crystal orientation anisotropy, the preferred orientation and the crystallite size in a welded steel plate [3]. However, the feasibility of this code has not been sufficiently confirmed yet. Therefore, we have compared the results obtained by the RITS code with those given by the Rietveld analysis software for neutron TOF diffractometry, and discuss the features of both transmission method and diffraction method.

2. RITS - A Rietveld-type analysis code for the Bragg-edge transmission imaging

The Rietveld analysis method [4] is a crystal structure analysis method for powder diffraction data of X-rays and neutrons. In this method, we calculate a whole scattering pattern based on the crystal structure factor, and

then refine the structural parameters by fitting the simulation calculation result to the experimental data by adjusting the parameters. The non-linear least-squares method, such as the Levenberg-Marquardt algorithm [5] used in the RITS code, has to be used for the adjustment of the non-linear parameters. Now, it is very important for the Bragg-edge transmission imaging to establish a theoretical model being able to correctly analyze the experimental data. Hereafter, we present the new theoretical expression of the Bragg-edge transmission spectrum to deduce the crystallographic and metallographic information.

The neutron transmission as a function of wavelength λ is related to the total cross section (the attenuation coefficient). The total cross section consists of elastic coherent scattering, elastic incoherent scattering, inelastic scattering and absorption parts. The elastic coherent scattering cross section $\sigma_{\mathrm{coh}}^{\mathrm{ela}}(\lambda)$ represents the Bragg-edge transmission profile. For developing the RITS code, we have proposed an effective formula that is composed of the kinematical diffraction theory [6] with three new factors: the Dreele-Jorgensen-Windsor type resolution function $R_{hkl}(\lambda,d_{hkl})$ [7] describing the edge asymmetric broadening for strain analysis, the modified March-Dollase function $P_{hkl}(\lambda,d_{hkl},R_0,HKL)$ [8] describing the crystal orientation anisotropy for texture analysis, and Sabine's extinction function $E_{hkl}(\lambda,F_{hkl},KD)$ [9] describing the re-diffraction phenomenon of diffracted neutrons inside one crystallite for microstructure analysis. This formula is expressed as follows:

$$\sigma_{\mathrm{coh}}^{\mathrm{ela}}(\lambda)=\frac{\lambda^2}{2V_0}\sum_{hkl}\left|F_{hkl}\right|^2 d_{hkl}R_{hkl}(\lambda-2d_{hkl})P_{hkl}(\lambda,2d_{hkl},R_0,HKL)E_{hkl}(\lambda,2d_{hkl},F_{hkl},KD)\ , \tag{1}$$

where V_0 is the unit cell volume of the crystal lattice, d_{hkl} is the distance of the crystal lattice plane $\{hkl\}$ (so-called the crystal lattice spacing or the d-spacing), and F_{hkl} is the crystal structure factor including the Debye-Waller factor. The first new factor, the Dreele-Jorgensen-Windsor type resolution function $R_{hkl}(\lambda,d_{hkl})$ [7], represents the edge asymmetric broadening due to the neutron pulse shape, the edge shift due to the macrostrain and the edge symmetric broadening due to the microstrain. The operation mode based on

the three-stage single edge profile analysis algorithm [10] has been optionally implemented in the RITS code for the high resolution strain imaging.

The second new factor, the March-Dollase function $P_{hkl}(\lambda,d_{hkl},R_0,HKL)$ [8], represents the crystal orientation distribution averaged over the Debye-Scherrer ring. Here, the March-Dollase coefficient R_0 means the degree of crystal orientation anisotropy. $R_0 = 1$ means that the orientation distribution is random (isotropic). As R_0 is away from unity, the anisotropy becomes large. The preferred orientation $<HKL>$ orients parallel to the incident beam direction when R_0 is less than one, and orients perpendicular to the incident beam direction when R_0 is greater than one. By using this function, we can calculate the shape change of the Bragg-edge transmission spectrum depending on the texture effect, and can deduce the orientation anisotropy factor R_0 and the preferred orientation $<HKL>$. The third new factor, Sabine's extinction function $E_{hkl}(\lambda,F_{hkl},KD)$ [9], represents the re-diffraction phenomenon of diffracted neutrons toward the transmitted beam direction occurring inside one crystallite (the primary extinction effect), and is formulated as a function of the crystallite size KD. By using this function, we can calculate the intensity increase of the Bragg-edge transmission spectrum depending on the extinction effect, and can deduce the crystallite size KD parallel to the transmitted beam direction.

3. Bragg-edge transmission imaging experiment with the RITS code

3.1 Specimens

Measured specimens were rolled and TIG (tungsten inert gas) welded low-carbon steel (α-iron) plates composed of body-centered-cubic (BCC) polycrystalline ferrites. Fig. 1 (a) shows a photograph of the specimens. Neutrons were transmitted through the normal direction (ND) in the top specimen, and were transmitted through the rolling direction (RD) in the bottom one. The weld zone exists along the center line. The neutron transmission thickness is 6 mm. Fig. 1 (b) shows stable end crystal orientations of a BCC metal after the rolling process. In general, the <111> orientation appears in the ND, and the <110> one appears in the RD [11]. In addition, we note that the grains in the weld zone are almost a half of the size of the grains in the base zone [3]. Thus, we have aimed at the quantitative

evaluation of the degree of crystal orientation anisotropy, the preferred orientation and the crystallite size in both the base zone and the weld zone, through the Bragg-edge transmission imaging with the RITS code.

Fig. 1. (a) Photograph of the specimens. (b) Typical stable end crystal orientations in the rolling process of a BCC polycrystalline material.

3.2 Experimental

A pulsed neutron TOF radiography experiment was carried out at the cold neutron beam-line at the electron linear accelerator facility at Hokkaido University in Japan. The neutron flight path length from the source to the detector was 6.03 m. The neutron flux at the detector position was about 10^3 n/cm^2/s. The neutron wavelength resolution and the d-spacing resolution was 2.7 % at the wavelength of 0.4 nm. The collimation ratio (L/D) was 60.3.

The two-dimensional neutron imaging detector used was a gaseous detector with GEM (gas electron multiplier) [12]. The position resolution was 800 μm. The detection area was 10 cm × 10 cm. The detection efficiency was 15 % at the neutron wavelength of 0.4 nm. The TOF resolution was 10 ns. The measurement time was 5.0 hours for the transmitted beam measurement, and was 3.3 hours for the incident beam measurement since we used a weak source and a detector with low detection efficiency.

3.3 Results and discussion

Fig. 2 shows four best fitting curves with each chi-square (χ^2) value indicating the goodness of the fitting, obtained by the RITS code. This figure also indicates their texture and microstructure parameters about the ND transmission data in the base zone, the ND transmission data in the weld zone, the RD transmission data in the base zone, and the RD transmission data in the weld zone. The experimental data plotted in Fig. 2 (and also Fig. 5) correspond to the data averaged over the pixels corresponding to the area of each specimen where the beams have been irradiated in the neutron diffraction experiment described later. These curves indicate that the implementation of the three new factors have worked well for reproducing the experimental data, and the RITS code can give the quantitative values of the

parameters of the preferred orientation, the crystal orientation anisotropy and the crystallite size.

Fig. 3 shows quantitative images of the degree of crystal orientation anisotropy R_0, the preferred orientation $<HKL>$ parallel to the neutron transmission direction and the crystallite size KD along the neutron transmission direction. Fig. 3 (a) indicates that the orientation anisotropies in the weld zone become random (isotropy) due to the rapid cooling and recrystallization during the solidification. Fig. 3 (b) indicates that the major preferred orientation along the ND is <111>, and the major preferred orientation along the RD is <110>. These are well consistent with the typical stable end orientation property of a rolled BCC metal. Fig. 3 (c) indicates that the crystallites in the weld zone become a half of the size of the crystallites in the base zone due to the rapid cooling and recrystallization during the solidification. This result is supported by the results of the grains observation using an optical microscope [3]. Thus, we have successfully evaluated the information on the texture and the microstructure by using the RITS code.

Fig. 2. Wavelength-dependent neutron transmission spectra of (a) the ND specimen and (b) the RD specimen, with the best fitting curves with each χ^2 value and the texture and microstructure parameters obtained by the RITS code.

Fig. 3. Quantitative images with respect to (a) the degree of crystal orientation anisotropy, (b) the preferred orientation parallel to the beam transmission direction and (c) the crystallites size along the beam transmission direction.

4. Comparison with the results of a neutron TOF diffraction experiment

4.1 Experimental

A pulsed neutron TOF diffraction experiment was carried out at the Ibaraki materials design diffractometer (iMATERIA) [13] at Materials and Life Science Experimental Facility (MLF) at Japan Proton Accelerator Research Complex (J-PARC) in Japan. The proton beam power was 120 kW during the

experiment. The d-spacing resolution is 0.16 % at the backward detectors bank. The time per once measurement was less than 1.0 hour. A diffraction pattern was integrated by the time-focusing method [14] in a scattering angle $2\theta > 150°$ of the backward detectors bank. We measured four kinds of diffraction pattern of the same zones as those measured by the transmission method as shown in Fig. 2.

4.2 Rietveld analysis results by using the Z-Rietveld code

We analyzed the experimental diffraction patterns by using the Z-Rietveld code [15] that is the Rietveld analysis software for pulsed neutron powder diffractometers installed at J-PARC. Fig. 4 shows a neutron TOF diffraction pattern with the best fitting curve in the ND of the base zone, and also the obtained texture and microstructure parameters. The isotropic displacement parameter of 0.292369×10^{-2} nm^2 was used and fixed during the Rietveld analyses. This value was equal to the value used in the analyses using the RITS code. It has been indicated by analyzing the four diffraction patterns that both the crystal orientation anisotropy and the crystallite size in the weld zone become smaller than those in the base zone (see also $R_{0,\mathrm{diff}}$ and KD_{diff} in Table 1). On the other hand, we have obtained the results as follows. The preferred orientation of the two ND specimens indicates that <530> is perpendicular to the beam direction since R_0 is greater than one, and the preferred orientation of the two RD specimens indicates that <530> is parallel to the beam direction since R_0 is less than one. Namely, the Z-Rietveld code has given an answer that the <530> orientation is parallel to the RD. This is quite different from the previous works in metallurgy and also the results of the Bragg-edge transmission imaging with the RITS code.

Fig. 4. Neutron TOF diffraction pattern of the ND of the base zone, the best Rietveld fitting curve provided by the Z-Rietveld code, and the obtained texture and microstructure parameters.

4.3 Discussion

The difference of the preferred orientation data may be caused by the time-focusing method. This is because this method averages and gradates

the preferred orientation effect during the focusing over the wide scattering angle (from 150° to 180° in this experiment). Therefore, we may obtain incorrectly the preferred orientation information in the neutron TOF diffraction experiment. For examining and preventing this phenomenon, we have to use an angle-dispersive neutron diffractometer at a steady neutron source.

For comparing the other parameters, the crystal orientation anisotropy R_0 and the crystallite size KD, we have re-analyzed the experimental transmission data shown in Fig. 2, under the condition that the preferred orientation <530> is assumed in the RITS code. Fig. 5 shows fitting results of the re-analyses with the χ^2 values. Table 1 shows the parameters obtained by the re-analyses ($R_{0,\mathrm{trans}}$ and KD_{trans}), and the results of the diffraction pattern analyses using the Z-Rietveld code ($R_{0,\mathrm{diff}}$ and KD_{diff}). The fitting curves shown in Fig. 5 are very close to the best fitting curves shown in Fig. 2 that the orientation <111> or <110> are identified as the preferred orientation. However, it is clearly indicated that the χ^2 values of Fig. 5 are worse than the χ^2 values of Fig. 2. This similarity may cause the difference of the results of the preferred orientation analyses between the transmission method and the diffraction method. Table 1 indicates that the crystal orientation anisotropies R_0 of both the transmission method and the diffraction method are close each other within 95 % ~ 99 %. On the other hand, the crystallite sizes of the transmission method KD_{trans} have been 1.52 ~ 1.58 times larger than the crystallite sizes of the diffraction method KD_{diff}. This indicates that the extinction function in the RITS code works stronger than the extinction function in the Z-Rietveld code. We should check the algorithms of both codes in detail for exploring the reason of this systematic difference.

Fig. 5. Fitting curves re-analyzed by the RITS code, assuming <530> as the preferred orientation. The χ^2 values in this figure are larger than those of the best fitting curves shown in Fig. 2.

Table 1. Comparison of the obtained parameters (crystal orientation anisotropy and crystallite size) between the transmission method and the

diffraction method. In the analyses using the RITS code, the preferred orientation has been fixed at <530> (the re-analysis results).

5. Conclusion

For quantitative visualization of texture and microstructure using a pulsed neutron Bragg-edge transmission imaging, we developed a Rietveld-type spectral fitting code, RITS, that is formulated by the kinematical diffraction theory and three new factors. By using the RITS code, we successfully obtained the quantitative images and the information on the crystal orientation anisotropy, the preferred orientation and the crystallite size in a welded α-iron plate, and they were well consistent with the previous works and the estimation by an optical microscope. For confirming the validity of the RITS code, we compared the results with those of a neutron TOF diffraction experiment. The trends of the results of the Rietveld analyses were consistent with those of the Bragg-edge transmission imaging with the RITS code, but some systematic differences existed on the preferred orientation and the crystallite size. We need to perform more detailed verification experiments by using an angle-dispersive diffractometer at a steady neutron source since the difference of the preferred orientation may be caused by the time-focusing of diffraction peaks. Furthermore, we need to check the algorithms of both the RITS code and the Z-Rietveld code in detail since the extinction function for crystallite size analysis is overvalued in the RITS code. Thus, the systematic studies are further required for the quantitative comparison of the obtained parameters between the transmission and the diffraction, and to confirm the feasibility of the pulsed neutron spectroscopic transmission imaging.

Acknowledgements

The authors are greatly thankful to the iMATERIA group of Ibaraki University for experimental assistance at J-PARC. This work was partially supported by Grant-in-Aid for Scientific Research (A) from Japan Society for the Promotion of Science (No. 20246136). H. Sato was supported by Grant-in-

Aid for JSPS Fellows from Japan Society for the Promotion of Science (No. 20002121).

References

[1] Y. Kiyanagi, N. Sakamoto, H. Iwasa, T. Kamiyama, F. Hiraga, S. Sato, H. Sagehashi, T. Ino, M. Furusaka, J. Suzuki, A. Gorin, I. Manuilov, A. Ryazantsev, K. Kuroda, K. Sakai, F. Tokanai, H. Miyasaka, T. Adachi, T. Oku, K. Ikeda, S. Suzuki, K. Morimoto and H.M. Shimizu, Some experimental studies on time-of-flight radiography using a pulsed neutron source, IEEE Trans. Nucl. Sci. 52 (2005) 371-374.

[2] H. Sato, O. Takada, K. Iwase, T. Kamiyama and Y. Kiyanagi, Imaging of a spatial distribution of preferred orientation of crystallites by pulsed neutron Bragg edge transmission, J. Phys. Conf. Ser. 251 (2010) 012070.

[3] H. Sato, T. Kamiyama and Y. Kiyanagi, A Rietveld-Type Analysis Code for Pulsed Neutron Bragg-Edge Transmission Imaging and Quantitative Evaluation of Texture and Microstructure of a Welded α-Iron Plate, Mater. Trans. (submitted).

[4] H.M. Rietveld, A profile refinement method for nuclear and magnetic structures, J. Appl. Crystallogr. 2 (1969) 65-71.

[5] D.W. Marquardt, An algorithm for least-squares estimation of nonlinear parameters, J. Soc. Indust. Appl. Math. 11 (1963) 431-441.

[6] E. Fermi, W.J. Sturm and R.G. Sachs, The transmission of slow neutrons through microcrystalline materials, Phys. Rev. 71 (1947) 589-594.

[7] S. Vogel, A Rietveld-Approach for the Analysis of Neutron Time-Of-Flight Transmission Data, Ph.D. Thesis, Christian Albrechts Universität, Kiel (2000).

[8] A.C. Larson and R.B. Von Dreele, General Structure Analysis System (GSAS), Los Alamos National Laboratory Report LAUR 86-748, Los Alamos National Laboratory, Los Alamos (2004).

[9] T.M. Sabine, R.B. Von Dreele and J.-E. Jørgensen, Extinction in time-of-flight neutron powder diffractometry, Acta Crystallogr. Sec. A 44 (1988) 374-379.

[10] J.R. Santisteban, L. Edwards, A. Steuwer and P.J. Withers, Time-of-flight neutron transmission diffraction, J. Appl. Crystallogr. 34 (2001) 289-297.

[11] H. Inagaki, Stable end orientations in the rolling textures of the polycrystalline iron, Z. Metallk. 78 (1987) 431-439.

[12] S. Uno, M. Sekimoto, T. Murakami, M. Tanaka, S. Nakagawa, E. Nakano, F. Sugiyama, K. Nagaya, A. Sugiyama and T. Uchida, Development of neutron gaseous detector with GEM, IEEE Nucl. Sci. Symp. Conf. Rec. 6 (2007) 4623-4626.
[13] T. Ishigaki, A. Hoshikawa, M. Yonemura, T. Morishima, T. Kamiyama, R. Oishi, K. Aizawa, T. Sakuma, Y. Tomota, M. Arai, M. Hayashi, K. Ebata, Y. Takano, K. Komatsuzaki, H. Asano, Y. Takano and T. Kasao, IBARAKI materials design diffractometer (iMATERIA) - Versatile neutron diffractometer at J-PARC, Nucl. Instrum. Methods Phys. Res. Sec. A 600 (2009) 189-191.
[14] J.D. Jorgensen, J. Faber Jnr, J.M. Carpenter, R.K. Crawford, J.R. Haumann, R.L. Hitterman, R. Kleb, G.E. Ostrowski, F.J. Rotella and T.G. Worlton, J. Appl. Crystallogr. 22 (1989) 321-333.
[15] R. Oishi, M. Yonemura, Y. Nishimaki, S. Torii, A. Hoshikawa, T. Ishigaki, T. Morishima, K. Mori and T. Kamiyama, Rietveld analysis software for J-PARC, Nucl. Instrum. Methods Phys. Res. Sec. A 600 (2009) 94-96.

CAPTION LIST

Fig. 1. (a) Photograph of the specimens. (b) Typical stable end crystal orientations in the rolling process of a BCC polycrystalline material.

Fig. 2. Wavelength-dependent neutron transmission spectra of (a) the ND specimen and (b) the RD specimen, with the best fitting curves with each χ^2 value and the texture and microstructure parameters obtained by the RITS code.

Fig. 3. Quantitative images with respect to (a) the degree of crystal orientation anisotropy, (b) the preferred orientation parallel to the beam transmission direction and (c) the crystallites size along the beam transmission direction.

Fig. 4. Neutron TOF diffraction pattern of the ND of the base zone, the best Rietveld fitting curve provided by the Z-Rietveld code, and the obtained texture and microstructure parameters.

Fig. 5. Fitting curves re-analyzed by the RITS code, assuming <530> as the preferred orientation. The χ^2 values in this figure are larger than those of the best fitting curves shown in Fig. 2.

CAPTION LIST

Table 1. Comparison of the obtained parameters (crystal orientation anisotropy and crystallite size) between the transmission method and the diffraction method. In the analyses using the RITS code, the preferred orientation has been fixed at <530> (the re-analysis results).

Figure-1

(a) Photograph of the specimens

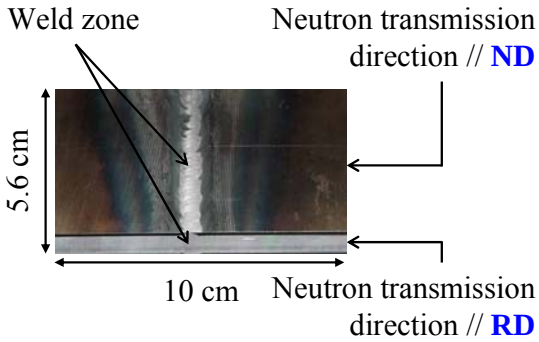

(b) Stable end crystal orientations in the rolling process of a BCC metal

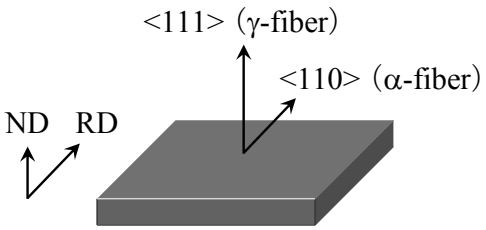

Figure-2

(a) Specimen of the normal direction

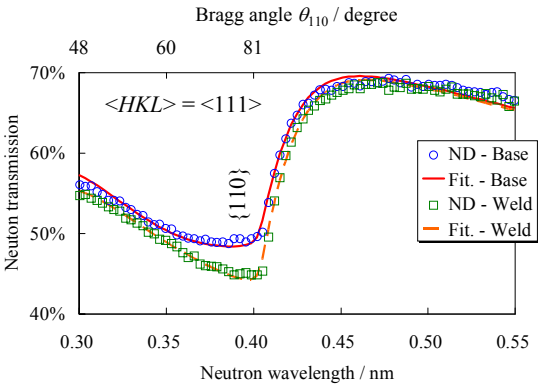

Base: $R_0 = 0.53$ & $KD = 4.58$ μm ($\chi^2 = 188.0$)
Weld: $R_0 = 0.63$ & $KD = 3.40$ μm ($\chi^2 = 123.4$)

(b) Specimen of the rolling direction

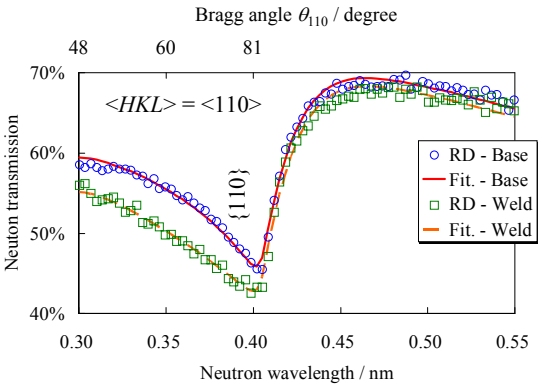

Base: $R_0 = 0.62$ & $KD = 5.44$ μm ($\chi^2 = 77.0$)
Weld: $R_0 = 0.73$ & $KD = 3.87$ μm ($\chi^2 = 52.2$)

Figure-3

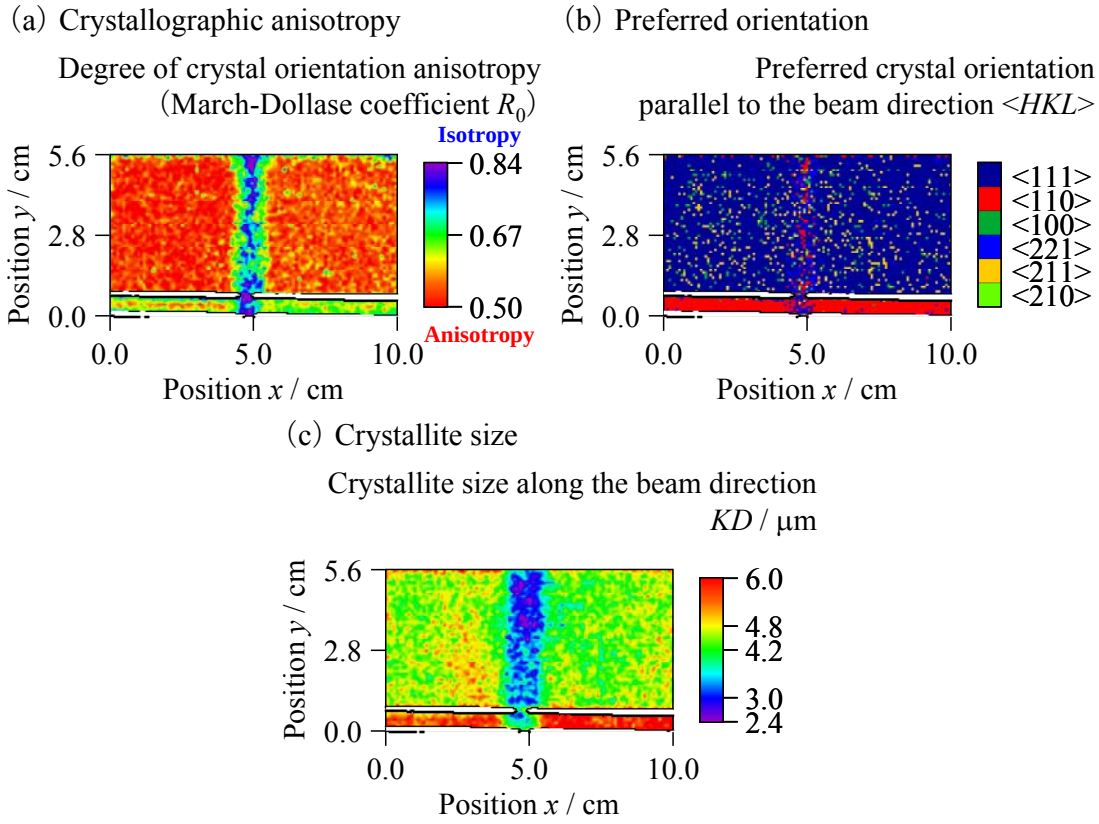
(a) Crystallographic anisotropy
Degree of crystal orientation anisotropy
(March-Dollase coefficient R_0)
Isotropy
0.84
0.67
0.50
Anisotropy
Position y / cm
5.6
2.8
0.0
0.0
5.0
10.0
Position x / cm
(b) Preferred orientation
Preferred crystal orientation
parallel to the beam direction <HKL>
<111>
<110>
<100>
<221>
<211>
<210>
(c) Crystallite size
Crystallite size along the beam direction
KD / μm
6.0
4.8
4.2
3.0
2.4

Figure-4

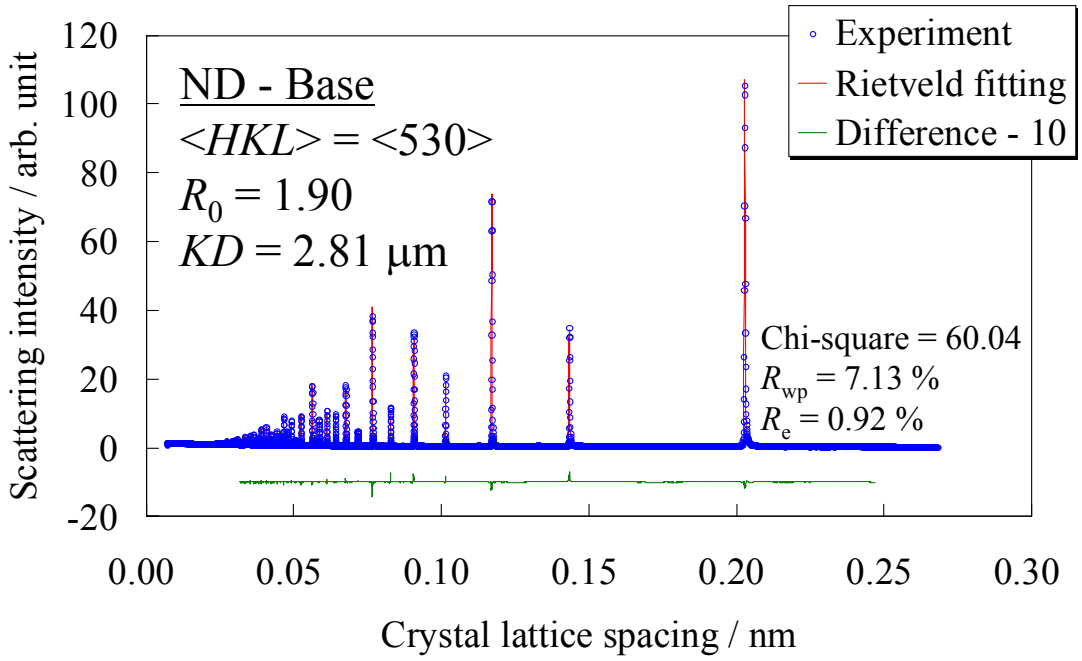
ND - Base
<HKL> = <530>
R0 = 1.90
KD = 2.81 μm
Experiment
Rietveld fitting
Difference - 10
Chi-square = 60.04
Rwp = 7.13 %
Re = 0.92 %
Scattering intensity / arb. unit
Crystal lattice spacing / nm
120
100
80
60
40
20
0
-20
0.00
0.05
0.10
0.15
0.20
0.25
0.30

Figure-5

(a) Specimen of the normal direction

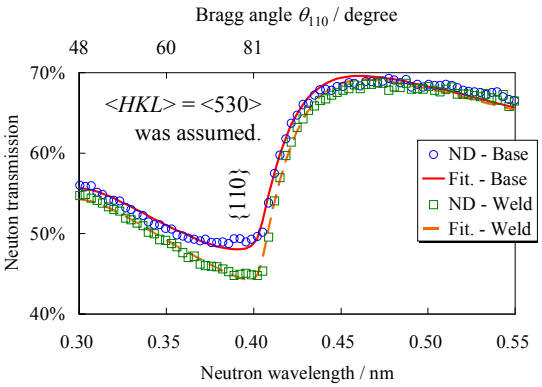

Base: R_0 = 1.85 & KD = 4.25 μm (χ^2 = 190.3)
Weld: R_0 = 1.51 & KD = 3.25 μm (χ^2 = 128.0)

(b) Specimen of the rolling direction

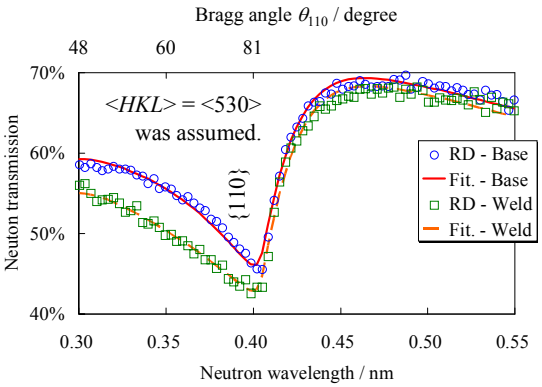

Base: R_0 = 0.54 & KD = 5.31 μm (χ^2 = 88.6)
Weld: R_0 = 0.66 & KD = 3.83 μm (χ^2 = 52.9)

Table-1

<*HKL*> = <530>	ND - Base	ND - Weld	RD - Base	RD - Weld
$R_{0,trans}$	1.846	1.514	0.538	0.655
$R_{0,diff}$	1.896	1.588	0.564	0.661
$R_{0,trans}$ / $R_{0,diff}$	97 %	95 %	95 %	99 %
KD_{trans}	4.25 µm	3.25 µm	5.31 µm	3.83 µm
KD_{diff}	2.81 µm	2.07 µm	3.37 µm	2.46 µm
KD_{trans} / KD_{diff}	152 %	157 %	158 %	155 %